ELSEVIER

0141-0296(96)00204-9

Engineering Structures, Vol. 18, No. 9, pp. 659–668, 1996

0141-0296/96 $15.00 + 0.00

Inelastic large deflection analysis of structural steel members under cyclic loading

Iraj H. P. Mamaghani, T. Usami and E. Mizuno

Department of Civil Engineering, Nagoya University, Chikusa-ku, Nagoya 464-01, Japan
(Received July 1995; revised version accepted October 1995)

The present paper is concerned with the cyclic inelastic large deflection analysis of structural steel members, such as pin-ended columns and fixed-ended tubular beam-columns of strut type. An elastoplastic finite element formulation for beam-columns, accounting for both the material and geometrical nonlinearities, was developed and implemented in the computer program FEAP used in the analysis. The geometrical nonlinearity is considered using the modified approximate updated Lagrangian description of motion. The two-surface plasticity model, recently developed by the authors, is employed for material nonlinearity. The model accounts for the important cyclic characteristics of structural steel, even within the yield plateau, such as, the decrease and disappearance of the yield plateau, reduction of the elastic range and cyclic strain hardening. The cyclic elastoplastic performance of the formulation was found to be good when compared with the experimental results as well as the results obtained from other material models. Copyright © 1996 Elsevier Science Ltd.

Keywords: inelastic, cyclic loading, large deflection, two-surface plasticity model, analysis, finite element, beam-columns

1. Introduction

Current seismic design philosophy relies strongly on the concept of energy dissipation through inelastic action. Steel braces are very effective structural members and are widely used as energy dissipaters in skeletal buildings and offshore structures under extreme loading conditions such as severe earthquake and wave motion. They also minimize storey drift of high-rise buildings for possible moderate earthquakes during their lifetime[1,2].

An accurate cyclic analysis of braced frames requires precise methods to predict the cyclic inelastic large deflection response of the braces. This has been the subject of intensive research work and a variety of analytical methods have been developed to simulate the hysteretic behaviour of braces in the past few decades[1–10]. An overview of Japanese research on steel braces has been given by Nakashima and Wakabayashi[11]. The main research approaches used for the cyclic analysis of braces may be classified as: empirical (phenomenological) models[3,4], plastic-hinge models[2,5,6] and elastoplastic finite element models[9,10].

The empirical models are based on simplified hysteretic rules that only mimic the experimental axial force–axial displacement relationship, and require numerous empirical input parameters for each member. To select such parameters one needs experimental results on braces similar to those under study[2]. In the plastic-hinge approach, it is assumed that the plastic hinges (instantaneous plastification) form at discrete points in the member, with the structure remaining elastic between the plastic hinges. Although the plastic-hinge method can provide a good insight into the basic hysteretic behaviour of a structure, a crucial drawback involved in this method is the neglect of gradual plastification through the cross-section and along the member length, the Bauschinger effect, cyclic strain hardening and residual stresses produced during hysteretic plastic deformation which are important factors in the overall response of the member[6].

The more accurate models were based on the finite element method considering geometric and material nonlinearities[10]. In this approach, the member is divided into several elements along its length, and the cross-sections are further subdivided into elemental areas to trace gradual plastification along the length and through the section of the member. This method is generally applicable to many types of problems, and it requires only the member

geometry and material properties (constitutive law) to be defined.

Recently, various stress–strain relationships have been employed in the analysis by different researchers, such as elastic-perfectly plastic, bilinear with hardening, and trilinear with both strain hardening and the Bauschinger effect[11]. From these studies, it was concluded that the spread of plasticity along the length and the Bauschinger effect cause a reduction in the maximum compressive resistance under cyclic loading[8]. On the other hand, the stress–strain relationship used in structural analyses depends on the loading history to which the structure or structural members are subjected. Therefore, an accurate and refined constitutive law should be used to account for the general cyclic behaviour of structural steel which has a characteristic yield plateau followed by strain hardening. For this purpose, based on the experimentally observed cyclic behaviour of structural steel, a multiaxial two-surface plasticity model (2SM) was recently developed by the authors[12–14]. This model can treat accurately the cyclic behaviour of structural steel even within the yield plateau, such as the reduction and disappearance of the yield plateau, the Bauschinger effect and cyclic strain hardening.

The main objective of this study is to apply the developed 2SM for material nonlinearity to trace the cyclic inelastic large deflection behaviour of structural bracing members, such as pin-ended columns and beam-columns of strut type. An elastoplastic finite element formulation for beam-column, considering geometrical and material nonlinearities, was developed and implemented in the computer program FEAP[15] used in the analysis. The modified approximate updated Lagrangian description (AULD) of motion[16] is adopted in the element formulation for geometrical nonlinearity.

In what follows, first the important characteristics of the uniaxial 2SM, numerical procedures and solution scheme are briefly presented. Then, the cyclic plasticity performance of the formulation is compared with experiments[3,17,18] as well as with results obtained from the elastic-perfectly plastic (EPP), isotropic hardening (IH) and kinematic hardening (KH) material models. It is found that the developed formulation can predict with a high degree of accuracy the experimentally observed cyclic behaviour of axially loaded pin-ended columns and beam-columns of strut type. Therefore, it can be used in the nonlinear structural analysis, to generate parametric data, and to check the accuracy of the more simplified models.

Also the effect of initial residual stress on the cyclic behaviour of steel columns is examined using the developed formulation. It is found that the initial residual stress has only the effect of decreasing the initial buckling load capacity and does not affect subsequent cyclic behaviour.

2. Review of the uniaxial two-surface model

The important characteristics of the uniaxial 2SM[12], shown schematically in *Figure 1*, are now briefly reviewed.

Plastic modulus: The same expression as in the Dafalias and Popov[19] model is used to calculate the plastic modulus E^p, that is

$$E^p = \frac{d\sigma}{d\epsilon^p} = E_0^p + h\frac{\delta}{\delta_{in} - \delta} \tag{1}$$

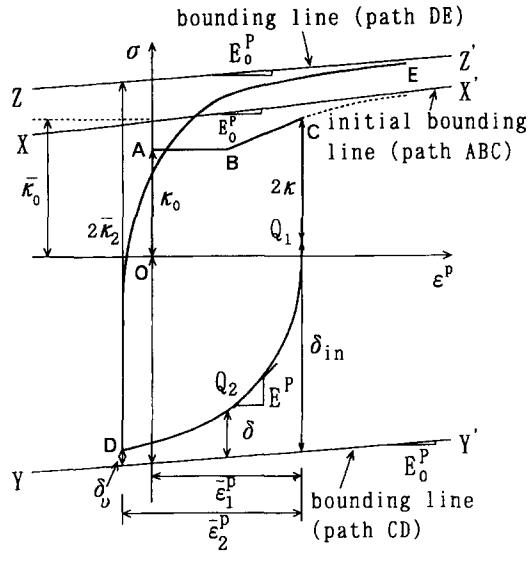

Figure 1 Uniaxial stress σ–plastic strain ϵ^p curve

where, E_0^p is the slope of the current bounding line defined in equation (7); δ is the distance between the bounding line and loading point (say, point Q_2 in *Figure 1*) and is assumed always greater than or equal to zero; δ_{in} is the value of δ at the initial yield state in the current loading path (say, point Q_1 for path CD in *Figure 1*); h is called the shape parameter and is assumed to be a linear function of δ as follows

$$h = e \cdot \delta + f \tag{2}$$

where e and f are material constants.

The plastic modulus E^p in equation (1), changes from infinity at the initial yield state $\delta = \delta_{in}$, to the slope of the bounding line, E_0^p, (see *Figure 1*), at the steady state $\delta = 0$, as δ decreases. This means that the transient elastoplastic behaviour under cyclic loading can be described by this model. Since at the initial yield state $\delta = \delta_{in}$, the denominator in equation (1) vanishes, this numerical problem can be overcome by setting the denominator to a very small value, say 1.0×10^{-8}, in the numerical analysis.

Reduction of the elastic range: The reduction of the elastic range (Bauschinger effect) is expressed as follows

$$\kappa/\kappa_0 = \alpha - a \cdot \exp(-b\bar{\epsilon}^p \times 100) - (\alpha - a - 1)\exp(-c\bar{\epsilon}^p \times 100) \tag{3}$$

where κ and κ_0 are half of the current and initial size of the elastic range, respectively ($\kappa_0 = \sigma_y$); a, b, c and α are constants; $\bar{\epsilon}^p$ is the effective plastic strain (EPS) range (denoted as AEPS by Shen *et al.*[12]), which is defined as the maximum amplitude of the effective plastic strain that the material has ever experienced.

Treatment of the yield plateau: The prediction of the end of yield plateau is important in the evaluation of cyclic behaviour. From the monotonic and cyclic experimental results, it is concluded that the disappearance of the yield plateau depends on the EPS range and the plastic work. The end of the yield plateau is judged by the following expression

$$\left(\frac{\bar{\epsilon}^p}{\epsilon^p_{st}} - 1\right) - m \cdot \left(\frac{W^P}{W^P_{st}} - 1\right) \begin{cases} < 0 & \text{yield plateau still continues} \\ \geq 0 & \text{yield plateau disappears} \end{cases} \quad (4)$$

where ϵ^p_{st} and W^P_{st} represent the plastic strain and plastic work at the end of the yield plateau under monotonic loading, respectively, W^P is the plastic work given by $\int \sigma d\epsilon^p$, and m is a material parameter.

The physical implication of equation (4) is that whether the material (steel) shows the hardening behaviour or not after the stress state reaches the yield stress σ_y[12]. That is, the hardening behaviour is assumed if a point $(W^P/W^P_{st}, \bar{\epsilon}^p/\epsilon^p_{st})$ lies above the line given by equation (4), otherwise the behaviour on the yield plateau is assumed.

Movement of the bounding line: The size of the bounding lines in the uniaxial case, $\bar{\kappa}$, is defined as a function of the EPS range, $\bar{\epsilon}^p$.

$$\bar{\kappa} = \bar{\kappa}_\infty + (\bar{\kappa}_0 - \bar{\kappa}_\infty) \exp(-0.25\zeta \bar{\epsilon}^{p^2}) \quad (5)$$

where $\bar{\kappa}_0$ is the size of the initial bounding line (see *Figure 1*); $\bar{\kappa}_\infty$ is the limiting value of the bounding line and assumed to be equal to the ultimate tensile stress σ_u; and ζ is the material constant.

Virtual bounding line and memory line: In order to predict random cyclic behaviour, the virtual bounding line and memory line concepts are proposed as shown in *Figure 2*. It is assumed that the virtual bounding line $X_v X'_v$, and memory line $X_m X'_m$ for the current loading path (path BC) are parallel to the real bounding line XX'. The initial memory line is assumed to pass the initial yield stress σ_y and moves together with the loading point A. Therefore, the loading point A on the memory line $X_m X'_m$ represents the point of the maximum stress that the material has ever experienced. Supposing that line $O_x O'_x$ is the centre line of the bounding lines XX' and YY', the memory lines $X_m X'_m$ and $Y_m Y'_m$ in tension and compression sides are assumed to be symmetrical with respect to this centre line $O_x O'_x$[12].

If the reversed loading point, such as point B in *Figure 2*, does not reach the memory line, the virtual bounding line $X_v X'_v$ will be used in the prediction of path BC. The virtual bounding line $X_v X'_v$ is assumed to shift up by a distance δ_v which is measured from the reversed loading point B to the memory line $Y_m Y'_m$. In the prediction of path BC, the plastic modulus E^P is calculated as

$$E^P = E^P_0 + h \frac{\delta + \delta_v}{\delta_{in} - \delta} \quad (6)$$

which is obtained by substituting $(\delta + \delta_v)$ and $(\delta_{in} + \delta_v)$ for δ and δ_{in}, respectively, in equation (1). However, once the loading point reaches the memory line $X_m X'_m$, such as point C in *Figure 2*, the plastic modulus in the continuous path CD is calculated by equation (1).

Slope of the bounding line: The slope of the current bounding line, E^P_0, is assumed to decrease with the plastic work W^P, and is expressed as

$$E^P_0 = \frac{E^P_{0i}}{1 + \omega W^P} \quad (7)$$

in which E^P_{0i} represents the slope of the initial bounding line determined from the monotonic loading experiment, where ω is a constant and W^P is the plastic work accumulated from the origin O to the current loading point.

It is worth noting that, in the proposed model, all the parameters are obtained from experimental data under relatively simple loading histories[12]. The material properties and model parameters for JIS SS400 steel (equivalent to ASTM A36), obtained by the authors, are listed in *Table 1*, where E and ν denote the Young's modulus and Poisson's ratio of the material, respectively.

In a work by the authors[13,14], by extending the effective plastic strain range concept into a multidimensional state, a generalized 2SM was developed for the multidimensional stress state. The accuracy of the 2SM has already been verified by the experimental data[12–14].

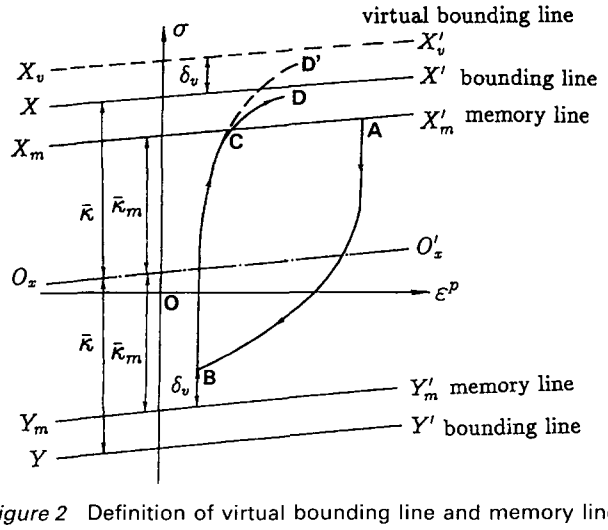

Figure 2 Definition of virtual bounding line and memory line

3. Numerical analysis procedure

In order to accurately consider the basic cyclic behaviour of structural steels in the analysis of structures or structural members, it is necessary to use an accurate constitutive law (stress–strain relationship) for the material. Therefore, an elastoplastic analysis based on the finite element method[10], which takes into account the spread of plasticity through the cross-section and along the length of member, is employed in the analysis of structural steel members, such as pin-ended columns and fixed-ended beam-columns of strut type. In this approach, the member analysed is divided into several elements along its length, and the cross-section is further subdivided into elemental areas, as shown in *Figure 3* for a hollow rectangular section. Each of the elemental areas is identified by, area dA_i, distance from the section centroid y_i, residual stress and strain, and stress–strain history. The incremental stress–strain relation for each elemental area is described by the developed 2SM discussed in the previous section. In the following discussion the element formulation for beam-columns is briefly presented.

3.1. *Beam-column element formulation*

The assumptions employed in the analysis are those of Bernoulli–Euler beam theory and the geometry within the

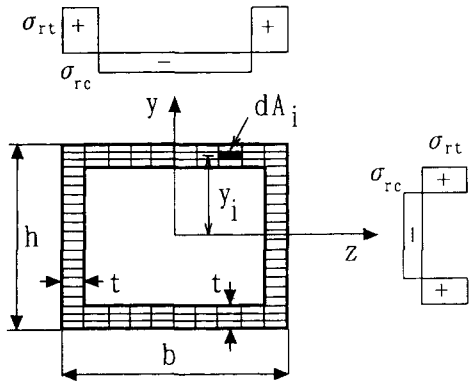

Figure 3 Subdivision of section and residual stress distribution for a hollow rectangular section

element is interpolated from the nodal parameters using Hermitian cubic shape functions[10]. In the present work, only longitudinal strain (ϵ_x) is considered and so at any point in the cross-section, yielding is assumed to occur as a result of longitudinal stress (σ_x) only. Local buckling is not considered in the analysis. The modified AULD of motion proposed by Jetteur *et al.*[16], is utilized in the element formulation. In this approach, beam elements are improved with the help of a Marguerre-type theory[20] which allows an introduction of initial deflections in the formulation and a reduction in the number of finite elements required to describe the nonlinear behaviour of the structure[16].

As shown in *Figure 4*, a local moving co-ordinate system (x_n,y_n) (rigid body motion co-ordinate) is applied to separate the real deformation of each element from its rigid body displacement[16]. It is assumed that the state of the element in the Ω_n configuration is known. A straight configuration Ω_n^*, joining the two end points of the deformed element, is taken as a reference configuration to define the configuration of the element in the subsequent step, Ω_{n+1}. The difference between Ω_n^* and Ω_n is considered as an initial deflection $\hat{v}(x)$ of the former. This gives rise to the modified version of the AULD that preserves the integration over a straight configuration Ω_n^*, and enables the curvature of the deformed configuration Ω_n[16] to be taken into account, as shown in *Figure 4*.

In the modified AULD, using the principle of virtual work in the local co-ordinate system and neglecting the transverse load, the linearized incremental equilibrium equation can be expressed as[16]

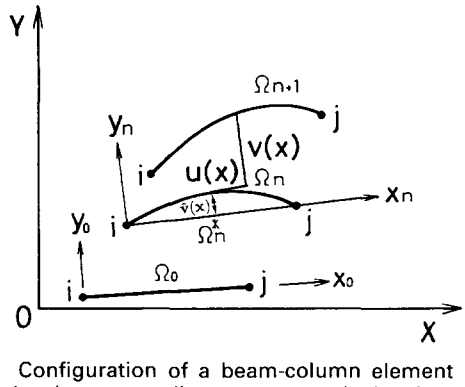

Figure 4 Configuration of a beam-column element in global *XY* and local *xy* co-ordinate systems (subscripts are step numbers)

$$\int_{V^*} \{\Delta\sigma\delta(\Delta e^L) + \sigma\delta(\Delta e^{NL})\}\, dV =$$

$$\{\delta(\Delta d)\}^T (\{\Delta\Gamma\} + \{\Gamma\}) - \int_{V^*} \sigma\delta(\Delta e^L)\, dV \qquad (8)$$

with

$$\{\Gamma\} = \{N_i, N_j, Q_i, M_i, Q_j, M_j\}^T \qquad (9)$$

$$\{d\} = \{u_i, u_j, v_i, \theta_i, v_j, \theta_j\}^T \qquad (10)$$

in which, as shown in *Figure 5*, $\{\Gamma\}$ and $\{d\}$, respectively, are nodal force and displacement vectors; σ denotes the axial Euler stress in the Ω_n^* configuration; e^L and e^{NL} are linear and nonlinear components of the axial Green's strain; Δ denotes the increment of the corresponding quantity; δ denotes 'variation in'; and V^* is the volume of element in the Ω_n^* configuration. u, v and θ are displacement components at nodal points and subscripts i and j denote nodal points. The incremental uniaxial stress–strain relationship is described by the developed 2SM as

$$\Delta\sigma = E_t \Delta e^L \qquad (11)$$

in which E_t is the current tangent modulus of the material.

The incremental axial displacement $\Delta u(x)$ and deflection $\Delta v(x)$ in an arbitrary section within the element is interpolated from nodal displacements using Hermitian cubic shape functions $[N_u]$ and $[N_v]$ as

$$\Delta u(x) = [N_u]^T \{\Delta d_u\} \qquad (12)$$

$$\Delta v(x) = [N_v]^T \{\Delta d_v\} \qquad (13)$$

in which

$$[N_u] = \begin{bmatrix} 1 - x/l_n \\ x/l_n \end{bmatrix} \qquad (14)$$

$$[N_v] = \begin{bmatrix} (1 + 2x/l_n)(1 - x/l_n)^2 \\ x(1 - x/l_n)^2 \\ 3(x/l_n)^2 - 2(x/l_n)^3 \\ -(l_n - x)(x/l_n)^2 \end{bmatrix} \qquad (15)$$

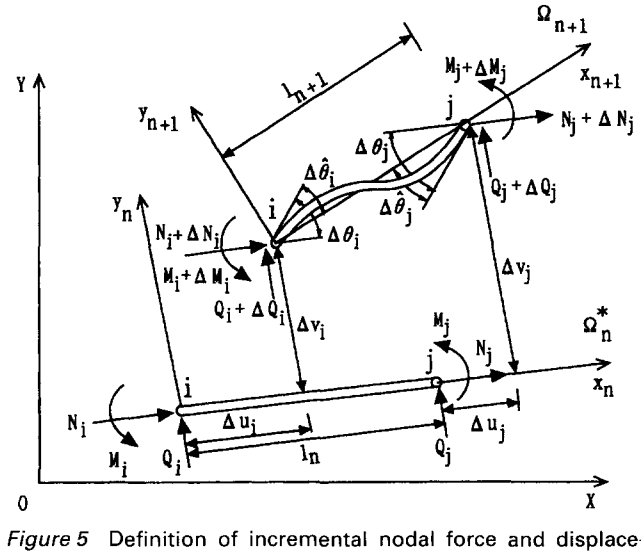

Figure 5 Definition of incremental nodal force and displacement vectors

l_n is the length of element in the Ω_n^* configuration; and $\{\Delta d_u\}$ and $\{\Delta d_v\}$ are components of the incremental nodal displacement vector $\{\Delta d\}$, i.e.

$$\{\Delta d\} = \{\{\Delta d_u\}^T, \{\Delta d_v\}^T\}^T \tag{16}$$

$$\{\Delta d_u\} = \{\Delta u_i, \Delta u_j\}^T \tag{17}$$

$$\{\Delta d_v\} = \{\Delta v_i, \Delta\theta_i, \Delta v_j, \Delta\theta_j\}^T \tag{18}$$

The incremental axial strain of an arbitrary point (elemental area) on the cross-section Δe can be expressed as the sum of linear and nonlinear components as

$$\Delta e = \Delta e^L + \Delta e^{NL} \tag{19}$$

The introduction of the initial deflection $\hat{v}(x)$ only modifies the linear part of the axial strain[16] so that

$$\Delta e^L = \Delta u'(x) - y\Delta v''(x) + \hat{v}'(x)\Delta v'(x) \tag{20}$$

and

$$\Delta e^{NL} = \frac{1}{2}\Delta u'(x)^2 + \frac{1}{2}\Delta v'(x)^2 \tag{21}$$

in which the primes denote the derivatives with respect to the column axis x; y is the co-ordinate of the centroid of the elemental area measured from the geometric centroid of the cross-section. Introducing equations (12) and (13) into equation (20) results in

$$\Delta e^L = [N_u']^T\{\Delta d_u\} - (y[N_v'']^T - \hat{v}'(x)[N_v']^T)\{\Delta d_v\} \tag{22}$$

where the initial deflection is defined in terms of the internal relative rotations at ends i and j with respect to the deflected chord of the element, $\Delta\hat{\theta}_i$ and $\Delta\hat{\theta}_j$ as shown in *Figure 5*, as follows

$$\hat{v}(x) = [N_v]^T\{0, \Delta\hat{\theta}_i, 0, \Delta\hat{\theta}_j\}^T \tag{23}$$

Making use of the above equations, the stiffness equation for the in-plane beam-column element in the local co-ordinate system can be written as

$$([k] + [k_G])\{\Delta d\} = \{\Delta\Gamma\} + \{\Gamma\} - \{f\} \tag{24}$$

with

$$[k] = \int_0^{l_n} \begin{bmatrix} k_{11} & k_{12} \\ \text{sym.} & k_{22} \end{bmatrix} dX \tag{25}$$

$$k_{11} = D_{11}[N_u'][N_u']^T$$
$$k_{12} = D_{12}[N_u'][N_v'']^T + D_{11}\hat{v}'(x)[N_u'][N_v']^T$$
$$k_{22} = D_{22}[N_v''][N_v'']^T + 2D_{12}\hat{v}'(x)[N_v''][N_v']^T \tag{26}$$

and

$$[k_G] = \int_0^{l_n} N \begin{bmatrix} k_{G11} & 0 \\ \text{sym.} & k_{G22} \end{bmatrix} dX \tag{27}$$

$$k_{G11} = [N_u'][N_u']^T$$
$$k_{G22} = [N_v'][N_v']^T \tag{28}$$

in which $[k]$ and $[k_G]$ are tangent and geometric stiffness matrices, respectively, N denotes axial load, and (D_{ij}, i,j = 1,2) can be written as

$$D_{11} = \int_A E_t dA \tag{29}$$

$$D_{12} = D_{21} = -\int_A E_t y dA \tag{30}$$

$$D_{22} = \int_A E_t y^2 dA \tag{31}$$

For the inplane analysis of beam-columns, a vector of equivalent nodal force vector $\{f\}$ can be derived as

$$\{f\} = \int_0^{l_n} \begin{Bmatrix} N[N_u'] \\ M[N_v''] + N\hat{v}'(x)[N_v'] \end{Bmatrix} dX \tag{32}$$

in which, the stress resultants of axial force (N) and bending moment (M) are obtained by

$$N = \int_A \sigma dA \tag{33}$$

$$M = -\int_A \sigma y dA \tag{34}$$

Using the cross-sectional subdivision the integrals in equations (29)–(31), (33) and (34) are calculated simply by summing the contribution of each elemental area over the cross-section. Once the stiffness matrix and nodal force vectors of each element are determined, they are rearranged according to the order of degree of freedoms for each node and transformed from the local to the global co-ordinate system using the usual transformation matrix.

3.2. Numerical integration and solution scheme

The Gauss–Lobatto numerical integration rule[21] is utilized in the present study to evaluate integrals in the stiffness equations. Five sample points are adopted. The modified Newton–Raphson iteration technique coupled with the displacement control method is used in the analysis. The details of the solution procedure can be found in Reference 22. The displacement convergence criteria is adopted in the analysis and the convergence tolerance is taken as 10^{-5}.

According to the algorithm discussed above, an elasto-plastic beam-column finite element subroutine program was coded and implemented in the computer program FEAP[15] used in the analysis.

4. Numerical examples

The developed formulation was used to predict the experimentally determined hysteretic behaviour of several steel columns and beam-columns of strut type subjected to cyclic

axial loading. The obtained results are also compared with those from the bilinear EPP, KH and IH material models. The aim is to compare the effect of each material model on the buckling and hysteretic behaviour of the structural members.

Based on the experimental results for SS400 steel, the kinematic and isotropic hardening rates are assumed as $d\sigma/d\epsilon^{p} = 0.00896E$ which is taken equal to the slope of the initial bounding line, E_{0i}^{p}, in 2SM (see *Table 1*). Initial residual stress is not considered in the analysis. An initial imperfection of $\delta(x) = \delta_0 \sin(\pi x/L)$ is assumed in the analysis of columns; where L and $\delta_0 = 0.1\%L$ stand for the length and initial deflection at midspan of the member, respectively. In the analyses, 10 elements have been used to discretize the member along its length and the cross-section is subdivided into 14 layers, parallel to the axis of bending, for prismatic solid rectangular sections and 48 (3×16 through thickness and radial, respectively) elemental areas for hollow circular sections. The compressive load is applied first and it is assumed to be positive.

4.1. *Pin-ended prismatic columns*

Pin-ended prismatic steel columns studied experimentally by Wakabayashi *et al.*[17] are analysed by using the theory and numerical procedure described. The first example is that of a column of effective slenderness ratio $KL/r = 40.46$, length $L = 174$ mm, width $b = 15.45$ mm and height $h = 14.90$ mm subjected to cyclic axial load, as shown in *Figure 6*. The specimen is made of SS400 steel with the properties of yield stress $\sigma_y = 229.0$ MPa, Young's modulus $E = 206.7$ GPa and yield plateau range $\epsilon_{st}^{p} = 0.8\%$.

Figure 6 compares the axial load–axial displacement and axial load–midspan deflection relationships obtained from experiment[17] and analysis using the 2SM as well as the EPP, KH and IH material models. In the following, some of the significant characteristics observed from the experimental and analytical results are pointed out and discussed.

As illustrated in *Figure 6a*, the experimentally observed complex cyclic behaviour in a typical hysteretic loop includes several characteristic stages: prebuckling (*OA*), postbuckling (*AB*), elastic unloading (*BC*), elastoplastic tensioning (*CDE*) and elastic unloading in tension side (*EF*). The first stage *OA* is associated with the initial compressive loading of a virgin column which buckles at point *A*. Stage *AB* is characterized by a decreasing axial load accompanied by column shortening. The shortening is primarily due to the formation of a lateral bow in the column [see *Figure 6b*(expt.[17])], which facilitates the through-section and along-length plastification of the member at midspan caused by the $P - v$ effect. Once the column

Table 1 Material properties and two-surface model parameters for steel grade JIS SS400

Parameter	Value	Parameter	Value
E(GPa)	204.0	σ_y(MPa)	260.0
ϵ_y	1.3×10^{-3}	ν	0.27
E_{st}^{p}/E	1.9×10^{-2}	ϵ_{st}^{p}	1.7×10^{-2}
a	−0.505	b	2.17
c	14.4	α	0.191
e	5.00×10^{2}	f/E	0.30
m	−0.37	E_{0}^{p}/E	8.96×10^{-3}
$\omega \cdot \sigma_y$	3.08	$\overline{\kappa}_0/\sigma_y$	1.15
σ_u/σ_y	1.67	$\zeta \cdot \epsilon_y^2$	9.89×10^{-4}

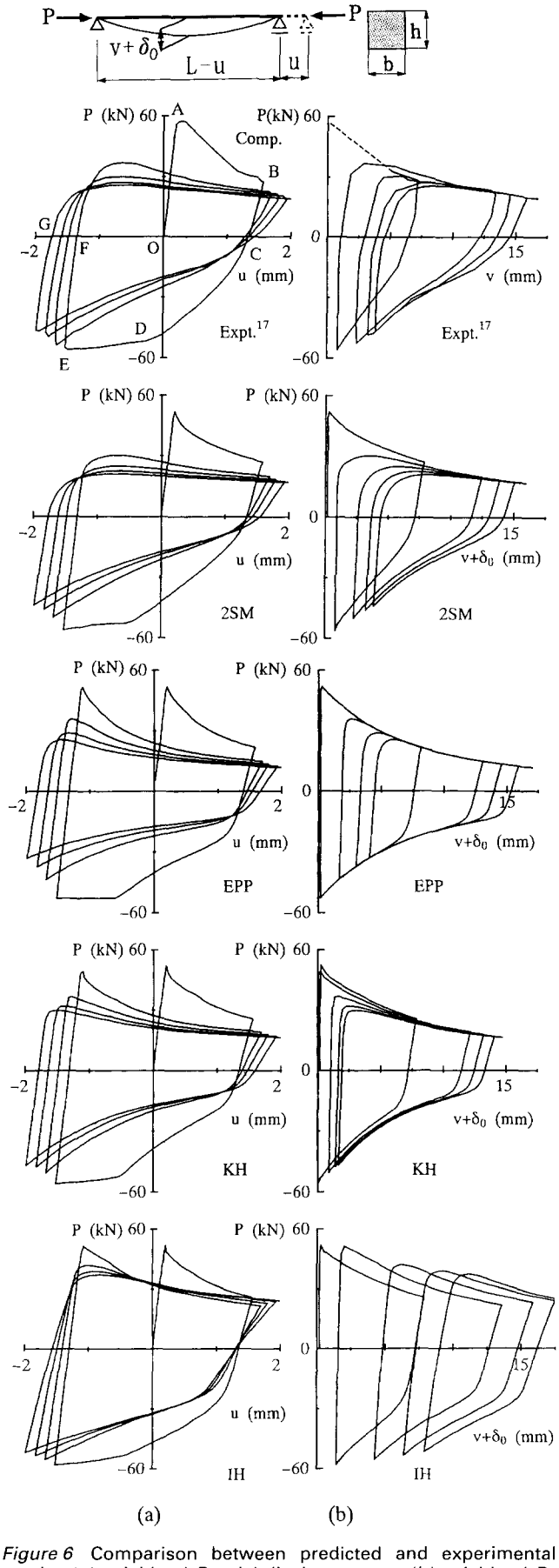

Figure 6 Comparison between predicted and experimental results: (a) axial load P–axial displacement u; (b) axial load P–midspan deflection v. ($KL/r = 40.46$, $L = 174$ mm, $b = 15.45$ mm, $h = 14.90$ mm, $\delta_0 = 0.1\%L$, $\sigma_y = 229.0$ MPa, $E = 206.7$ GPa, $\epsilon_{st}^{p} = 0.8\%$)

begins to buckle, plastic deformation rapidly develops, and the axial force decreases with the axial displacement u, which is kinematically related to the lateral deflection v.

Stage BC is the elastic unloading of the column. The slope of this line is less than that for stage OA, since the stiffness of a member with a larger bow in it is smaller than that for a smaller bow due to the initial imperfection. During the application of a tensile force of an increasing magnitude, curve CDE in *Figure 6a*, the column elongates and gradually straightens as shown in *Figure 6b* for the experiment. Along the curve CD, it is difficult to separate the Bauschinger effect and the effect of gradual straightening of the column which have softening and stiffening effects on the curve, respectively. However, the general trend of the influence is that the Bauschinger effect becomes pronounced, initially, owing to the associated reduction in tangent modulus, and later the straightening effect of the column prevents softening of the curve caused by the spread of plasticity. This trend is more apparent in the same stage for the subsequent cycles, as can be noticed in *Figure 6a*. Stage DE corresponds to the fully yielding of the column at midspan. Due to the strain hardening of the material, the line DE develops a positive slope. The axial deformation is reversed at point E and the member behaves elastically until point F, at which one cycle is executed. At point F the axial load is zero, but residual axial deformation (elongation of the member, see *Figure 6a*) and curvature (midspan deflection as shown in *Figure 6b*), as well as residual stresses and strains exist in the member. These effects are taken into consideration in the prediction of the subsequent cycles in the analysis. The general characteristics of the subsequent hysteretic loops, for a cyclically loaded column, are the same as the first cycle except for the following observations.

(1) The maximum compressive load decreases with subsequent cycles of loading [see *Figure 6a*(expt.)]. The decrease in the second cycle is much greater than that of subsequent cycles, in which the hysteresis loops tend to be stabilized with a few cycles. This is attributed to the presence of a residual lateral deflection at the midspan of the member, as shown in *Figure 6b*. Moreover, since the column at midspan experiences severe stress reversals, the material undergoes strain hardening. However, the influence of the Bauschinger effect on reducing the tangent stiffness of the member plays a more dominant role than the strain hardening, owing to the associated lower values of the tangent modulus in comparison with the elastic modulus of the steel in a virgin state. Consequently, there is a greater propensity for buckling to occur.

(2) As shown in *Figure 6a*(expt.), the column is progressively lengthened from point F to point G due to the successive loading cycles which follow compressive ones.

(3) *Figure 6a* shows that the postbuckling curve in the first cycle is steeper than that of the second and subsequent cycles in the experiment. This observation indicates that the postbuckling behaviour is sensitive to the strain hardening effect of the material which is induced following the disappearance of the yield plateau caused by accumulated plastic work at the midspan of the column.

Figure 7 compares the change in load carrying capacity of the column during cyclic loading obtained from experiment and analyses. With reference to *Figures 6* and *7*, the following observations can be made. (1) The initial buckling load (see *Figure 7*) is slightly higher in the experiment than that predicted by the analyses using different material

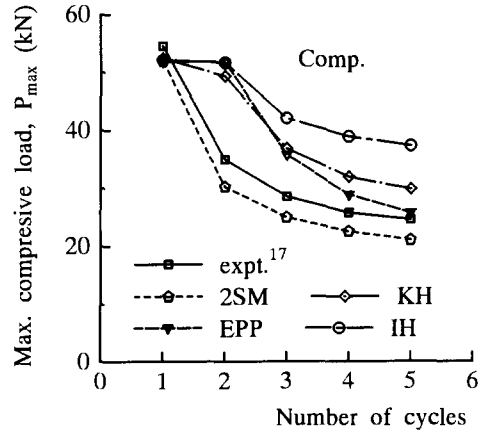

Figure 7 Change in load carrying capacity during cyclic loading. (key as in *Figure 6*)

models. This may be due to the experimental boundary conditions (unavoidable friction at the hinged supports) and the assumed initial imperfection in the analysis. (2) The significant features of the hysteretic loops in *Figure 6a* is that all of the models except the 2SM give the second and subsequent buckling load capacities higher than those of the experiment (see also *Figure 7*). The reasons are: firstly, the EPP and IH models do not consider the reduction of the elastic range due to plastic deformation (Bauschinger effect); and for the KH model the size of the elastic range is taken to be constant which does not represent the actual behaviour of the structural steel[12]. In the case of the 2SM this effect is accurately taken into account through equation (3), which has the effect of softening the hysteresis curve (reduction in stiffness), leading to a lower value of the buckling load capacity. And, secondly, the 2SM correctly treats the yield plateau and cyclic strain hardening of the material. This leads to an accurate prediction of the axial load–midspan deflection [see *Figure 6b*(2SM)] for the column, since the residual deflection of the column at the end of the previous tensioning has a large effect on the buckling load capacity and subsequent cyclic behaviour. As can be noticed from *Figure 6b*, the progress of buckling is different for each material model. In the case of the IH model, in spite of large progress in buckling (see *Figure 6b*), the buckling load capacity does not decrease significantly due to the larger cyclic strain hardening.

As shown in *Figures 6* and *7*, the 2SM predicts all of the above discussed experimentally observed hysteretic behaviour of the column much better than the other material models.

Figures 8 and *9* compare the experimental[17] and analytical (2SM) axial load–axial displacement and axial load–midspan deflection relationships for the pin-ended prismatic columns of effective slenderness ratios $KL/r = 80.23$ and 120.66, respectively. As shown in these figures, the predicted results are quite close to the experimental data, and similar observations as in the previous example can be made.

At this point it is interesting to note that Nonaka[23] also attempted to predict the hysteretic behaviour of a pin-ended prismatic column subjected to repeated axial loading, using a general elastic-plastic solution. Elastic-perfectly plastic behaviour was assumed in the analysis under the combined action of axial force and bending moment. Consequently, despite the simplicity of the solution, it has a demerit in the prediction that a plastically deformed column completely

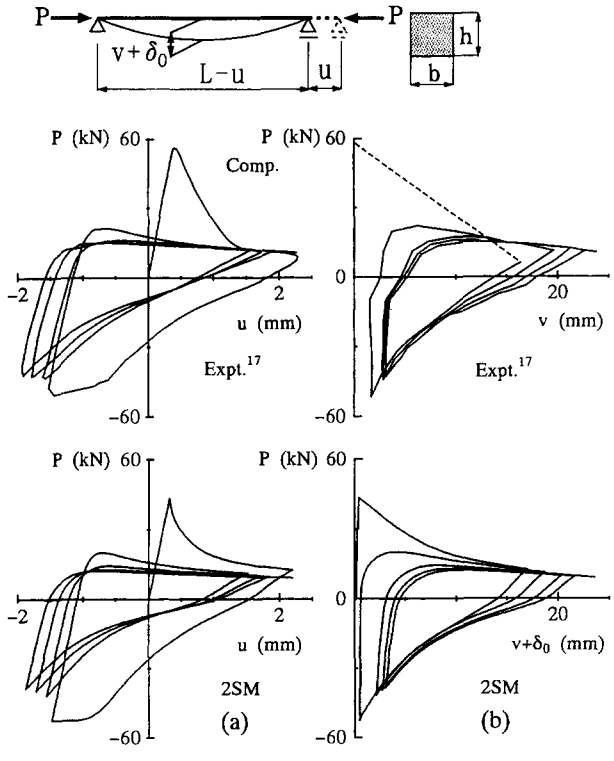

Figure 8 Comparison between predicted and experimental results: (a) axial load P–axial displacement u; (b) axial load P–midspan deflection v. ($KL/r = 80.23$, $L = 349$ mm, $b = 15.21$ mm, $h = 15.07$ mm, $\delta_0 = 0.1\%L$, $\sigma_y = 229.0$ MPa, $E = 206.7$ GPa, $\epsilon^p_{st} = 0.8\%$)

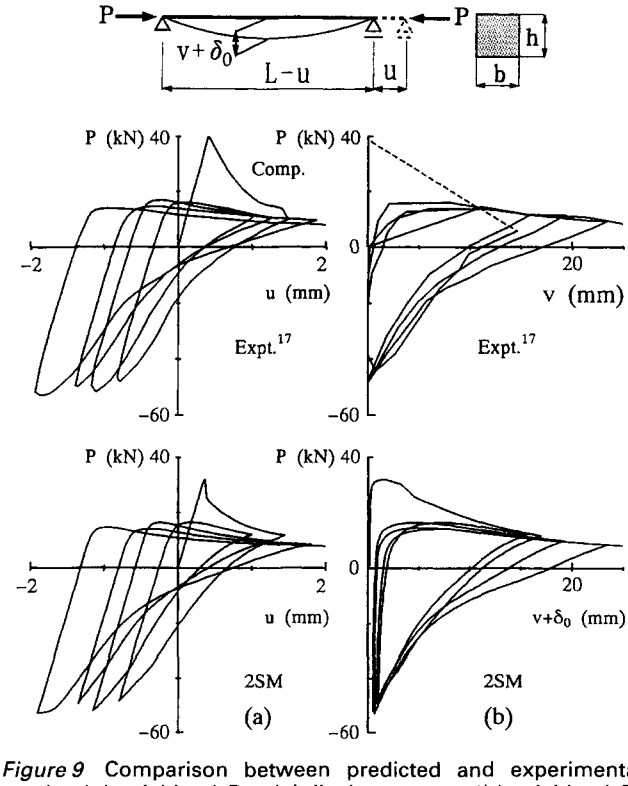

Figure 9 Comparison between predicted and experimental results: (a) axial load P–axial displacement u; (b) axial load P–midspan deflection v. ($KL/r = 120.66$, $L = 521$ mm, $b = 15.42$ mm, $h = 14.96$ mm, $\delta_0 = 0.1\%L$, $\sigma_y = 229.0$ MPa, $E = 206.7$ GPa, $\epsilon^p_{st} = 0.8\%$)

restores its full strength and initial straightness upon the reversion of the axial displacement[23], due to the neglect of the spread of plasticity, Bauschinger effect and strain hardening of the material. This is in contrast to the actual observation that a plastically deformed column hardly becomes straight again through mere extension[23]. This disadvantage has been overcome by the developed formulation (2SM) as discussed above.

4.2. *Pin-ended tubular column*

Figure 10 compares the experimental[3] and analytical axial load–axial displacement hysteretic behaviour for a pin-ended tubular column of effective slenderness ratio $KL/r = 115$, length $L = 2300$ mm, outer diameter $D = 60.33$ mm and wall thickness $t = 3.91$ mm. The specimen has material properties of yield stress $\sigma_y = 379.0$ MPa and Young's modulus $E = 197.0$ GPa. As can be seen from *Figure 10*, the load carrying capacity rapidly decreased after the initial buckling due to yielding of the section at midspan of the specimen. The buckling continues until an axial shortening of 82 mm occurs, giving rise to 350 mm lateral deflection in the experiment. The corresponding lateral deflection predicted by the 2SM is 300 mm. The large reduction in the buckling load capacity is observed in both experiment and prediction in the second cycle. As can be seen in *Figure 10*, the developed formulation using the 2SM predicts the experiment quite well.

4.3. *Tubular beam-columns of strut type*

Beam-columns of strut type are fixed-ended bracing members subjected to constant lateral loads Q, and cyclic axial displacements u, (see *Figure 11*)[1]. These members are widely used in offshore steel platforms and space truss structures. The cyclic behaviour of the struts has been the subject of intensive research in recent years. Among others, they have been studied experimentally by Sherman[18] and theoretically by Chen and Han[1,7]. The loading conditions, cross-sectional properties and dimensions of the struts reported in Reference 1 are used in the present study.

Using the developed formulation (2SM), a series of numerical studies on the cyclic behaviour of struts are carried out and the results are compared with the test data[18].

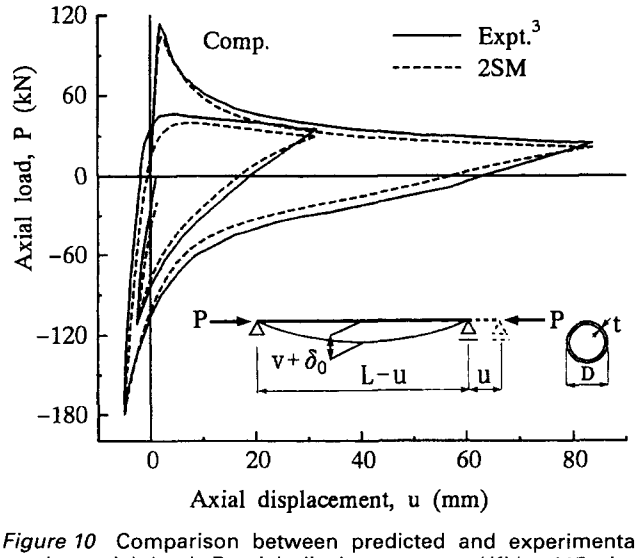

Figure 10 Comparison between predicted and experimental results; axial load P–axial displacement u. ($KL/r = 115$, $L = 2300$ mm, $D = 60.33$ mm, $t = 3.91$ mm, $\delta_0 = 0.1\%L$, $\sigma_y = 379.0$ MPa, $E = 197.0$ GPa)

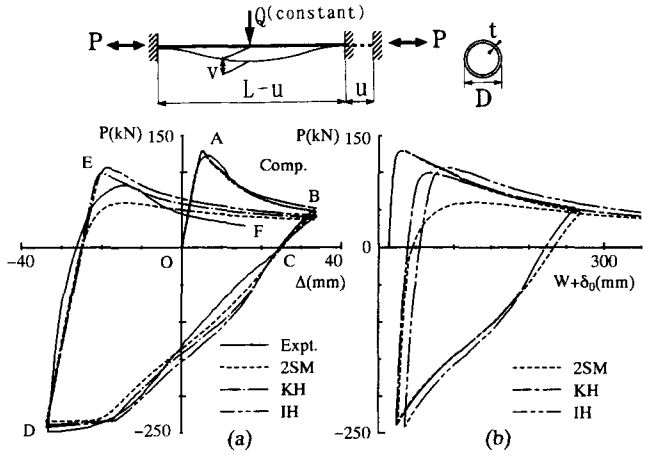

Figure 11 Comparison between predicted and experimental results: (a) axial load P–axial displacement u; (b) axial load P–midspan deflection v. ($KL/r = 72$, $L = 5720$ mm, $D = 114.0$ mm, $t = 2.3$ mm, $\sigma_y = 289$ MPa, $Q = 0.4Q_y$, $Q_y = 9.12$ kN, $E = 200.0$ GPa)

Figures 11 and *12* show axial load–axial shortening and axial load–midspan deflection for two typical examples, with material constants, dimensions, boundary and loading conditions as shown (see captions of *Figures 11* and *12*). The specimens have an effective slenderness ratio of $Kl/r = 72$ and are subjected to lateral load ratios of $Q/Q_y = 0.4$ and 0.2, respectively. Q is the lateral point load and Q_y is the value of Q which causes first yield in a strut with no axial load applied. An initial imperfection and residual stress are not considered in these examples.

After applying the constant lateral load of Q at midspan, the specimen is first loaded in compression. The 2SM, KH and IH models simulate the experiments quite well in the pre- and post-buckling stages of axial deformation (for example, see path OAB in *Figure 11*). Upon reversal of the axial deformation in tension (path BCD) and reloading in compression (path DEF), the 2SM provides a relatively closer fit to the test data as compared with the other models, owing to the same reasons mentioned in the previous examples. As shown in *Figures 11* and *12*, except for the 2SM the buckling load capacity in the second cycle is predicted to be higher than that of the experiments (i.e. at point E in *Figure 11*).

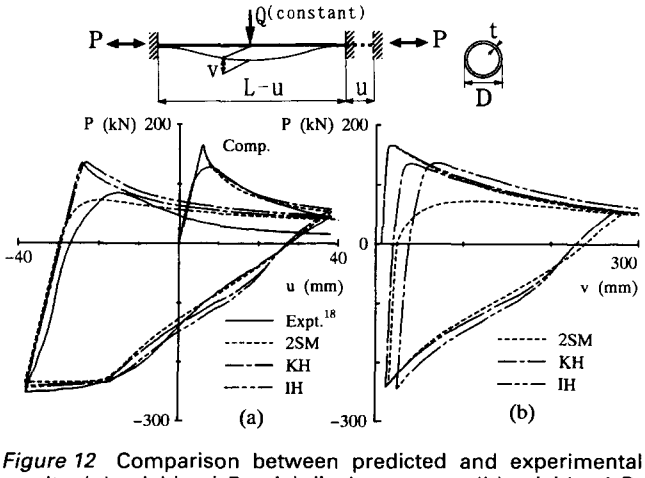

Figure 12 Comparison between predicted and experimental results: (a) axial load P–axial displacement u; (b) axial load P–midspan deflection v. ($KL/r = 72$, $Q = 0.2Q_y$) (key as in *Figure 11*)

5. Effect of residual stress

The effect of residual stress on the cyclic behaviour of steel members is examined using the developed formulation. As a typical example, the effect of longitudinal residual stresses produced due to welding (it is assumed that the specimen is built up by welding of four plates), on the cyclic behaviour of a pin-ended column with a hollow rectangular section is shown in *Figure 13*. The member of effective slenderness ratio $KL/r = 70$, length $L = 3150$ mm, width $b = 150$ mm, height $h = 110$ mm and wall thickness $t = 4.5$ mm was subjected to cyclic axial loading. The material was assumed to be SS400 steel with yield stress $\sigma_y = 265.9$ MPa, Young's modulus $E = 197$ GPa, and a yield plateau range $\epsilon^p_{st} = 10\epsilon_y$. The cross-section was subdivided into 30 (3×10) and 15 elemental areas in the flanges and webs, respectively (*Figure 3*). The assumed residual stress distribution over the cross-section is also shown in *Figure 3*, and is uniform along the entire length on the member. The tensile and compressive residual stresses are taken as $\sigma_{rt} = \sigma_y$ and $\sigma_{rc} = 0.4\sigma_y$, respectively.

The normalized axial load P/P_y–axial displacement u/u_y relationship, shown in *Figure 13*, indicates that the initial buckling load capacity decreases by 15%, from $P/P_y = 0.84$ (corresponding $u/u_y = 0.846$) to $P/P_y = 0.71$ ($u/u_y = 0.910$), due to residual stresses. Here, P_y is the squash load and u_y is the yield displacement in tension for the column. The obtained results indicate that the residual stresses have almost no effect on the subsequent cyclic behaviour of the column, (see *Figure 13*). (Also, experimental studies on the inelastic behaviour of steel frames subjected to vertical and monotonic lateral loading, reported by Wakabayashi *et al.*[24], indicate that annealing does not affect overall frame behaviour.)

From the mechanical point of view these observations can be explained as follows. Residual stresses cause the fibres with an initial compressive stress to yield before the applied stress reaches the yield strength of the material. Then, yielding spreads progressively without significant strain hardening due to the existence of the yield plateau,

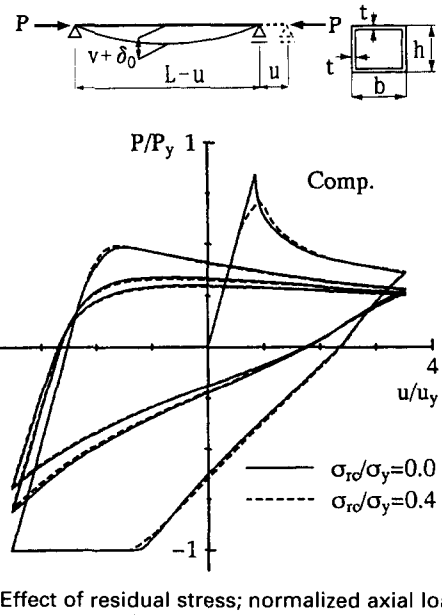

Figure 13 Effect of residual stress; normalized axial load P/P_y–axial displacement u/u_y for a pin-ended tubular column. ($KL/r = 70$, $L = 3150$ mm, $b = 150.0$ mm, $h = 110.0$ mm, $t = 4.5$ mm, $\delta_0 = 0.1\%L$, $\sigma_y = 265.9$ MPa, $E = 197$ GPa, $\epsilon^p_{st} = 10\epsilon_y$, $\sigma_{rt} = \sigma_y$ and $\sigma_{rc} = 0.4\sigma_y$)

as the load increases monotonically before unloading starts. Initially, this causes a reduction in compressive strength of the member, while later both of the response curves, with and without residual stress, almost coincide as can be seen in *Figure 13*. At this stage, the residual stresses produced due to plastic deformation play a dominant role in the subsequent cyclic behaviour of the column as compared to the initial residual stresses. That is, the effect of initial residual stresses on the subsequent cyclic behaviour significantly decreases (see *Figure 13*).

6. Conclusions

The present paper is concerned with the cyclic inelastic large deflection analysis of structural steel members, such as pin-ended columns and beam-columns of strut type. An elastoplastic finite element formulation for beam-columns, accounting for both the material and geometrical nonlinearities, was developed and implemented in the computer program FEAP used in the analysis. The geometrical nonlinearity was considered using the modified approximate updated Lagrangian description of motion. The 2SM, recently developed by the authors, was employed for material nonlinearity. The model accurately takes into account the experimentally observed cyclic behaviour of structural steel, even within the yield plateau which is an important characteristic of this material, the decrease and disappearance of the yield plateau, reduction of the elastic range, and cyclic strain hardening.

The cyclic elastoplastic performance of the formulation was compared with the experimental results as well as with those obtained using the EPP, KH and IH material models. It was shown that:

- The formulation is applicable for any geometry of the cross-section and takes into account the spread of plasticity and history-dependent parameters which are important for the accuracy of the analysis.
- The results obtained indicate that the reduction of the elastic range has a significant effect of reducing the maximum compressive resistance under load reversals.
- The residual deflection (progress in buckling) of the steel members at the end of previous tensioning has a large effect on the reduction of the buckling load capacity and subsequent cyclic behaviour. This behaviour is accurately predicted by the developed formulation.
- The proposed formulation accurately takes into account the important cyclic characteristics of axially loaded columns and beam-columns, such as yielding in tension and buckling under compression, inelastic behaviour prior to buckling in compression, degradation of postbuckling compressive resistance, deterioration of buckling load capacity in subsequent inelastic cycles, progressive degradation of tangent modulus during the cycles, and plastic elongation in the column length.
- The predicted hysteretic behaviour of structural steel members using the 2SM was in good agreement with the experimental results compared with the EPP, KH and IH models.
- The initial residual stress significantly decreases the initial buckling load capacity and has almost no effect on the subsequent cyclic behaviour of the column.

Comparison between the experimental results and predictions indicates that these observations can be mainly attributed to the accuracy of the 2SM employed in the analyses. This leads to the conclusion that the 2SM is quite promising to account for the material nonlinearity of structural steels under cyclic loading. Therefore, it can be used in the nonlinear structural analysis; to generate parametric data; and to check the accuracy of more simplified models.

References

1 Han, D. J. and Chen, W. F. 'Behavior of portal and strut types of beams-columns', *Engng Struct.* 1983, **5**, 15–25
2 Soroushian, P. and Alawa, M. S. 'Efficient formulation of physical theory brace models', *J. Struct. Engng, ASCE* 1988, **114** (11), 2457–2473
3 Maison, B. F. and Popov, E. P. 'Cyclic response prediction for braced steel frames', *J. Struct. Engng, ASCE* 1980, **106** (7), 1401–1416
4 Jain, A. K., Goel, S. C. and Hanson, R. D. 'Hysteretic cycles of axially loaded steel members', *J. Struct. Engng, ASCE* 1980, **106** (8), 1777–1795
5 Toma, S. and Chen, W. F. 'Cyclic analysis of fixed-ended steel beam-columns', *J. Struct. Engng, ASCE* 1982, **108** (6), 1385–1399
6 Boutros, M. K. 'Nonlinear SDOF element for hysteretic analysis of pinned braces', *J. Engng Mech., ASCE* 1991, **117** (5), 941–953
7 Chen, W. F. and Han, D. J. '*Tubular members in offshore structures*', Pitman Publishing Inc, 1985
8 Shibata, M. and Wakabayashi, M. 'Mathematical expression of hysteretic behaviour of braces: part 2: application to dynamic response analysis', *Trans. Arch. Inst. Japan*, October 1982, No. 320, 29–35 (in Japanese)
9 Chan, S. L. and Kitipornchai, S. 'Inelastic postbuckling behaviour of tubular struts', *J. Struct. Engng, ASCE* 1988, **114** (5), 1091–1105
10 Clarke, M. J. 'Plastic-zone analysis of frames', in *Advanced analysis of steel frames*, W. F. Chen and S. Toma (Eds) CRC Press, Boca Raton, FL, 1994, pp 259–319
11 Nakashima, M. and Wakabayashi, M. 'Analysis and design of steel braces and braced frames in building structures' in *Stability and ductility of steel structures under cyclic loading*, Y. Fukumoto and G. C. Lee (Eds) CRC Press, Boca Raton, FL, 1992, pp 309–321
12 Shen, C., Tanaka, Y., Mizuno, E. and Usami, T. 'A two-surface model for steels with yield plateau', *J. Struct. Engng/Earthquake Engng, JSCE* 1992, **8** (4), 179–188
13 Mamaghani, I. H. P., Shen, C., Mizuno, E. and Usami, T. 'Cyclic behaviour of structural steels, I: experiments', *J. Engng Mech., ASCE* 1995, **121** (11), 1158–1164
14 Shen, C., Mamaghani, I. H. P., Mizuno, E. and Usami, T. 'Cyclic behaviour of structural steels, II: theory', *J. Engng Mech., ASCE* 1995, **121** (11), 1165–1172
15 Zienkiewicz, O. C. '*The finite element method*' (3rd edn) McGraw-Hill, New York, 1977
16 Jetteur, Ph., Cescotto, S., de Ville de Goyet, V. and Frey, F. 'Improved nonlinear finite elements for oriented bodies using an extension of Marguerre's theory', *Comput. Struct.* 1983, **17** (1), 129–137
17 Wakabayashi, M., Nonaka, T., Koshiro, O. and Yamamoto, N. 'An experiment on the behaviour of a steel bar under repeated axial loading', Disaster Prevention Research Institute Annuals, Kyoto University, Kyoto, Japan, 1971, No. 14 A, 381–381 (in Japanese)
18 Sherman, D. R. 'Post local buckling behaviour of tubular strut type beam-columns: An experimental study', Report to Shell Oil Company, University of Wisconsin-Milwaukee, June 1980
19 Dafalias, Y. F. and Popov, E. P. 'A model of nonlinear hardening materials for complex loading', *Acta Mech.* 1975, **21**, 173–192
20 Washizu, K. '*Variational methods in elasticity and plasticity*' (3rd edn) Pergamon Press, 1982
21 Hughes, T. J. R. '*The finite-element*', Prentice-Hall, Englewood Cliffs, NJ, 1987
22 Ge, H. B. and Usami, T. 'Development of earthquake-resistant ultimate strength design method for concrete-filled steel structures', NUCE Research Report, No. 9401, Nagoya University, Japan, 1994
23 Nonaka, T. 'Approximation of yield condition for the hysteretic behavior of a bar under repeated axial loading', *Int. J. Solids Struct.* 1977, **13**, 637–643
24 Wakabayashi, M., Nonaka, T. and Matsui, C. 'An experimental study on the inelastic behavior of steel frames subjected to vertical and horizontal loading', *Bull. Disas. Prev. Res. Inst., Kyoto Univ.*, Kyoto, Japan, 1967, Vol. 17, Part 1, No. 119, 28–48